International Journal of Basic Science and Technology
May, Volume 10, Number 2, Pages 146 - 158 http://www.ijbst.fuotuoke.edu.ng/ 146
https://doi.org/10.5555/IEMP4633 **ISSN 2488-8648**

Numerical Computation of Effective Dielectric Constant on the Skin

Adebayo, A.D. and Ifeagwu, E. N.

Department of Electrical and Electronic Engineering, Federal University Otuoke, Bayelsa State Nigeria

Article Information

Article # 10019
Received: 20th Sept. 2023
1st Revision:4h Jan. 2024
2nd Revision:6th March 2024
Acceptance:29th April 2024
Available online:
3rd May 2024.

Abstract

The effective dielectric constant on human skin, a critical characteristic in many biological and communication applications, is the subject of this research and is computed numerically. We study the intricate relationship between electromagnetic fields and skin tissues using sophisticated computational models and simulation approaches to precisely calculate the effective dielectric constant. The study's conclusions offer insightful information for improving the functionality and design of skin-based technology, including communication systems, wearable sensors, and medical equipment.

Key Words: Computational Models, Simulations, Dielectric, Communication Systems, electromagnetic fields

***Corresponding Author:** Adebayo, A.D.; adebayoad@fuotuoke.edu.ng

Introduction

Understanding how electromagnetic radiation interacts with the human body is crucial for determining the safety of electromagnetic field exposure for humans as well as for a wide range of biomedical applications. This can be achieved through measuring the dielectric characteristics of tissues. The dielectric characteristics of different tissues have been measured and modeled in several studies (Peyman, 2011). A well-known work on this subject by Gabriel *et al.* (2016a) published two decades ago, includes a parametric model that specifies tissue properties in the 10 Hz–20 GHz range and a large database based on impedance measurements. Over time, this database has come to be widely recognized as a standard resource for figuring out a tissue's dielectric characteristics. Skin is one of the few tissues in this database that has two separate conductivity and permittivity values given for it. The values specified in the database for both wet and dry skin are two orders of magnitude different, suggesting that the skin's dielectric characteristics are highly dependent on the environment in which it is found. As such, the particular application for which the measurements are being conducted as well as the environment that this application places on the skin must be taken into account when measuring the dielectric properties of skin. A unique anticancer therapeutic approach that has arisen recently is called tumor treating fields, or TTFields. is a noteworthy application that necessitates a thorough comprehension of the skin's dielectric characteristics in the intermediate frequency region. Low-intensity alternating electric fields, or TTFields, have an antimitotic effect on malignant cells when applied in the 100–500 kHz frequency range (Kirson et al 2007, Giladi *et al.*, 2015). GBM patients can receive TTFields therapeutic approval from the Food and Drug Administration (FDA). Furthermore, there are ongoing clinical trials examining the viability, security, and effectiveness of TTFields in treating lung cancer (NCT02973789), pancreatic cancer (NCT01971281), mesothelioma (NCT02397928), ovarian cancer (NCT02244502), hepatocellular carcinoma (NCT03606590), and other conditions for which strong preclinical data support additional clinical research (Davies *et al.*, 2013, Giladi *et al.*, 2014, Voloshin et al 2016, Karanam *et al.*, 2017).

Non-invasive diagnosis is becoming more common in clinical practice, primarily to lower the risk of infection and allow for ongoing monitoring while also improving patient comfort. Since the cell shape is subsequently modified with advancing precancerous stage, skin cancer, skin irritations, ischemia detection, measurement of oedema in irritant-exposed skin, monitoring of in vitro tissue engineering, or tumor characterization, dielectric spectroscopy and electric impedance spectroscopy are already used for inspection of cervical squamous tissue. To examine individual cells at the microscopic level, specialized dielectric spectroscopy-based methods including electrorotation, dielectrophoresis, and impedance flow cytometry are used. One potential use is the monitoring of physiologically-induced alterations in dielectric characteristics to analyze blood parameters. Nevertheless, the difficulties with these measures are comparable to those encountered with other medical applications like EEG, EMG, etc. that involve placing electrodes on the skin. The skin is a layered, lossy

https://doi.org/10.5555/IEMP4633 ISSN 2488-8648

tissue with extremely different material compositions in each of its sublayers, which gives it unique dielectric characteristics. Apart from the skin's inherent structure, Dielectric readings are influenced by several factors such as the electrode skin and contact. It becomes more difficult to use numerical modeling to address the aforementioned problems. A precise solution to the forward problem is essential to extracting any desired parameters from the measured data. The dielectric properties of the top layer, the stratum corneum (SC), epidermis, dermis, and hypodermis have not yet been measured in vivo using skin with and without this top layer. There is currently no complete (continuous) set of these properties available in the frequency range between 1 and 100 MHz. Coaxial probes with varying diameters were used to identify the SC, and permittivity estimates for the epidermis/dermis and hypodermis (subcutaneous fat), but only for single frequencies. Using a coaxial probe and the time domain reflectometry (TDR) approach, two relaxation processes in the microwave frequency region were identified and quantified in addition to measuring powdered native SC. Measurements of the in vivo skin, blood, infiltrated, and non-infiltrated fat were made, and Cole–Cole relaxation models were generated for each substance that was measured.

The permittivity of biological tissue can be tested using many of the same methods and ideas as conventional engineering materials. The tissue's capacitance is first measured, and using the relationship between the electromagnetic theory and tissue morphology, permittivity can then be computed based on the test results. In other words, calculations based on test results (capacitance) are used to conduct an experimental investigation on the permittivity of biological tissue. Many specific applications have already been reflected in the research that is already available.

According to Otaki *et al*. (2017), a dielectric blood coagulometer could be a valuable technique for gauging blood clotting and could offer a comprehensive evaluation of the state of anticoagulant therapy. The dielectric properties of biological systems are unstable and vary depending on external factors like temperature and external electric frequency. The dielectric characteristics of living tissue are unique, and the computation of effective permittivity through theory modeling can significantly lessen the effort involved in investigating them (Huclova *et al.*,2010). Numerous theoretical research has already been conducted on the simulation of effective permittivity in biological tissue utilizing various methods such as the finite element approach, effective medium approximation, and perturbation expansion. The majority of research on mathematical models of tissue permittivity employed the composite material model.

In a 2014 study by Bagnaninchi et al., measurements of human skin were made in vivo, along with a Cole-Cole fit. The Cole–Cole fits are a well-liked and practical method for characterizing the dielectric spectra of tissue in general, as noted in Cowen *et al.*, (2014).

Materials and Methods

The cell shape has a significant influence on the effective dielectric properties at frequencies <10 MHz to be able to decide which features are necessary to be included in an appropriate skin model, detailed knowledge of the skin morphology is required. The Skin cell contains flat hexagonally shaped corneocytes embedded in a lipid matrix forming a so-called 'bricks-and-mortar' structure. The diameter of a corneocyte is 40 μm, and the height is 0.8 μm. The intercellular distance is approximately 0.1 μm which provides a cellular volume fraction of $\phi_{\text{corneocyte}} = 0.85$. The cytoplasm contains ceramides, free fatty acids, cholesterol, proteins (keratin) and water. In contrast to most other cells the corneocyte does not contain a nucleus.

The extracellular matrix, the 'mortar' mainly consists of lipids and proteins and very little bound water (less than a monolayer). The total water volume fraction in the SC is 0.15–0.25, while 90% of the water is contained within the corneocyte. By definition, the SC belongs to the epidermis, but due to the high lipid and protein and low water content, it differs significantly from the lower-lying epidermal layers and is here therefore considered separately. The SC thickness depends on the body site but exhibits only little interindividual variations among healthy subjects. On the dorsal site of the upper arm, the SC is approximately 20 μm thick. The living epidermis (E) mainly consists of keratinocytes. The cuboidal to columnar epidermal cells are gap-connected and occupy a volume fraction of 0.83. The overall water volume fraction in the dermis of 0.7 is equally distributed among intra- and extracellular space. The epidermis is approximately 0.1–0.2 mm thick. The transition zone between epidermis and dermis (D), the so-called dermo-epidermal junction, is not planar but forms papillae with a depth of 50 μm. The papillary dermis (PD) occupies the upper 10% of the dermis and consists of a dense collagen network and blood ($\phi_{\text{blood}} = 0.04$). The major part of the dermis, the reticular dermis (RD) consists of irregular connective tissue, lymphatic vessels, nerves, blood vessels, stromal cells

https://doi.org/10.5555/IEMP4633 ISSN 2488-8648

such as fibroblasts and other cellular components, e.g., macrophages or plasma cells. The capillaries in the approximately 200 μm long dermal papillae are oriented perpendicular to the skin surface, while the upper vessel plexus (UVP) is a dense vascular network.

Assessment of Body Impedance in Patients

In this investigation, we evaluated the average electric impedance among pancreatic cancer patients receiving TTFields treatment. Based on data from 19 pancreatic cancer patients treated with TTFields as a part of the PANOVA trial (NCT0197128), the analysis was conducted (Rivera *et al.*,2019). Every thirty minutes, the voltage, current, and absolute electric impedance of patients receiving TTFields therapy are recorded. The purpose of this record is to allow the treating physician to evaluate patient adherence to treatment guidelines and the effectiveness of the treatment.

Measuring the Dielectric Properties of Skin

To estimate the dielectric properties of skin, we measured the complex impedance of skin folds around the waists of volunteers (two males and three females). To ensure that the conditions of the skin resembled the conditions when TTFields are delivered to a patient, the impedance measurements were performed using electrodes made of ceramic disks and medical gels (Axelgaard AG625) similar to those present in the TAs used to deliver TTFields. The electrodes were placed on both sides of a skin fold at five to six different locations around the waists of the volunteers. The folds and the electrodes were held in place by a clamp to maintain geometry and pressure during the measurement. A schematic diagram illustrating the measurement setup is shown in figure 2(a). Measurements were taken at room temperature and skin temperature was 30 °C–32 °C. The thickness of each fold was measured using a caliper and documented. Complex impedance was recorded at multiple frequencies in the range of 100kHz to 1 MHz using a Keysight E4980AL Precision LCR Meter. With this setup, measuring the impedance of a single skin fold took approximately 1 min. After every measurement, the combined impedance of the ceramic disks and gel was measured by sandwiching the layers of gel between the ceramic disks and connecting.

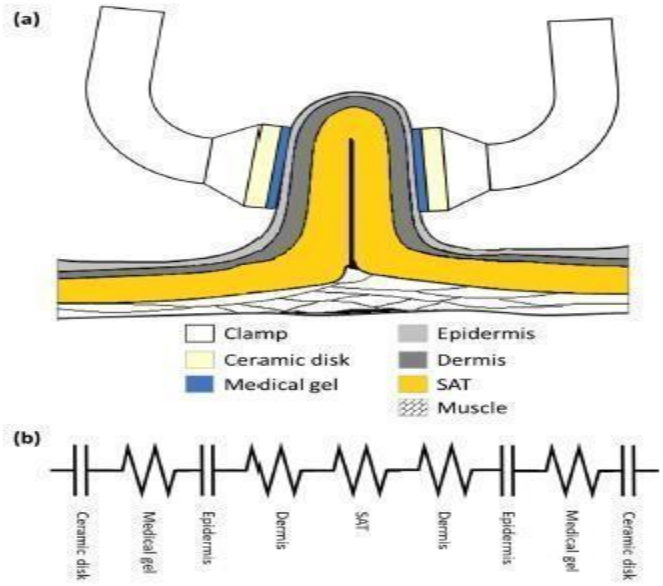

Figure 1. (a) Skin fold impedance measurement setup: electrodes made of ceramic disks and medical hydrogel placed on either side of a skin fold (epidermis, dermis, and SAT). (b) Multilayer electric circuit model of a skin fold measurement with five tissue layers: epidermis (capacitive); dermis (resistive); SAT (resist

Modeling and Analysis of the Impedance Measurements

According to the geometry of the measurement setup, only the outer layers of the body are sandwiched between two parallel electrodes (figure 3.1(a)). In the structure that is formed in the fold, all layers have almost uniform cross-sections and are connected in series. Consequently, a simple multilayer model can be used to analyze the measurements. The multilayer model of the skinfold used for analysis included five layers of tissue: epidermis, dermis, SAT, dermis and epidermis sandwiched between two layers of medical

https://doi.org/10.5555/IEMP4633 ISSN 2488-8648

gel, and two ceramic disks, as shown in figure 3.1(b). The dermis and SAT layers were considered mainly resistive due to their relatively high water content and their low relative permittivity as reported in the literature (Gabriel et al 1996c). The epidermis was considered to behave as a capacitor due to its thinness and very low water content, which correlate with high relative permittivity and extremely low conductivity. Using this model, the complex impedance Z for any measurement can be expressed as:

$$Z = Z_{RE} + iZ_{IM} \quad (3.1)$$

$$ZZ_{RE} = Z_S + 2Z_d = \frac{I_S}{\sigma_S A} + 2.\frac{I_d}{\sigma_d A} \quad (3.2)$$

$$Z_{IM} = -\frac{I_E}{\varepsilon 0 \varepsilon r A \omega} \quad (3.3)$$

$$I_t = I_S + I_d + I_e \quad (3.4)$$

Equations (3.1)– (3.4) show that the real and imaginary components of the tissue impedance, ZRe and ZIm, respectively, depend on six variables: the thickness of the SAT (ls), the thickness of the dermis (ld), the thickness of the epidermis (le), the total thickness of the fold (lt), the conductivities of the SAT (σs) and the dermis (σd), and the relative permittivity of the epidermis (εr). Two constants present in the equations are the vacuum permittivity ε0 = 8.85 · 10−12 F m−1 and the cross-section of the layers A. This analysis assumes that the measurement geometry resembles a parallel plate setup in which all layers have the same cross-section as the electrodes. However, during the measurements, the skin fold was stretched to be slightly larger than the electrodes to ensure perfect contact between the medical gel and the skin surface. In addition, the skin fold is connected to a larger body and current can flow through the inner tissues, which may slightly change the uniform cross-section geometry. Therefore, when deriving dielectric properties from the measurement data, it is important to use an effective cross-section area, Aeff, which is different from the cross-section area of the electrode and links the realistic skin fold geometry with the multilayer model. Details on how Aeff was derived are explained in the next section. It is reasonable to assume that variations in the thicknesses of skin folds are caused primarily by changes in the thickness of SAT at different locations on a single individual and between individuals and that changes in the thicknesses of the epidermis and dermis are very small relative to changes in the thickness of the SAT.

Therefore, we assume constant thicknesses of le = 80 · 10−6 m for the epidermis (Zolfaghari and Maerefat, 2010) and ld = 2 · 10−3 m for the dermis. Thus, the relative permittivity of the epidermis can be derived from equation (3.5) by isolating εr:

$$\varepsilon_r = \frac{l_e}{|Z_{\mathrm{Im}}|\,\varepsilon_0 A_{eff}\omega}. \quad (3.5)$$

Here, ZIm is the average of the imaginary component of the impedance measured for all skin fold samples. To calculate the conductivity of SAT and the dermis layers, we applied equation (3.4) into (3.2), which after neglecting the epidermis thickness yields:

$$Z_{\mathrm{Re}} = \frac{1}{\sigma_s A_{eff}} \cdot l_t + \left(\frac{2\sigma_s - \sigma_d}{\sigma_s \sigma_d A_{eff}}\right) \cdot l_d. \quad (3.6)$$

This equation shows that it is possible to derive values for the conductivity of the SAT and dermis by plotting the real part of the skin fold impedance as a function of total skin fold thickness lt, and performing a linear regression on the plot. Analyzing the slope and intercept coefficients derived from the regression (m and n, respectively) yields the conductivity of the SAT and dermis:

https://doi.org/10.5555/IEMP4633 ISSN 2488-8648

$$\sigma_s = \frac{1}{mA_{eff}} \tag{3.7}$$

$$\sigma_d = \frac{2 \cdot l_d \sigma_s}{\sigma_s A_{eff} n + l_d}. \tag{3.8}$$

These values were reassigned into the computational model to yield another modification to Aeff. We continued this iterative process of correcting the effective area and dielectric values until the simulation yielded an effective area with corresponding calculated dielectric properties that were within 2% of the dielectric values assigned in that simulation. Convergence occurred after three to four iterative steps. The simplified skin fold measurement model used for this process is shown in Figure 3.1 The model comprised a large box (40cm × 15cm × 20cm) representing the torso, with a smaller box attached to the center of one of the faces, representing a skin fold. The small box comprised three segments: epidermis, dermis, and SAT with thicknesses of 0.1mm, 2mm, and 9.8mm, respectively (figure 3(b)). The size of the fold along the Z-axis was 4cm and the size of the fold pulled outward from the body was 3.5cm.

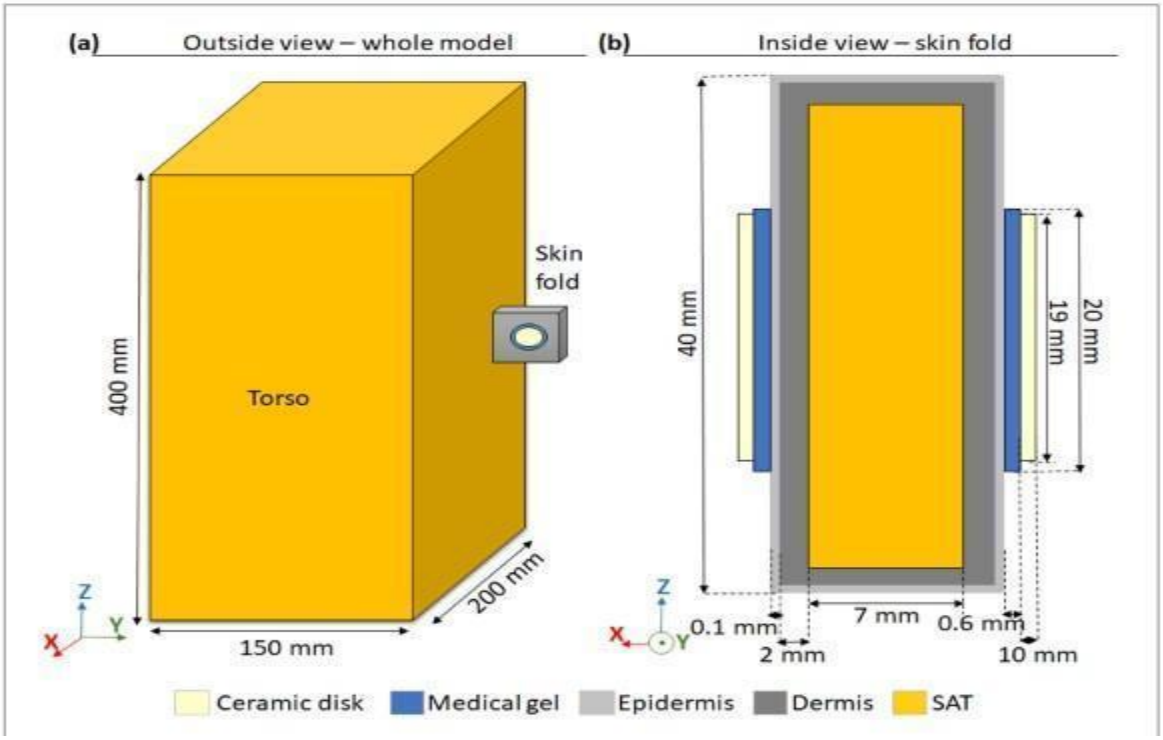

Fig 2: The large box representing the torso of two tissue types

The large box representing the torso comprised only two tissue types: SAT as the outermost layer (7mm thickness) and muscle tissue filling the inner volume. We set the dielectric properties assigned to the epidermis, dermis, and SAT according to the iterative process described in the previous paragraph and the dielectric properties of the inner large box were approximated to those of muscle as reported in the IT'IS database 3.1.1 (Hasgall *et al.*, 2015). A ceramic disk (19mm in diameter, 1mm thick) was attached to each side of the fold through a cylindrical gel (20mm in diameter, 0.6mm thick) that adhered to the fold's surface (figure 3(b)). The dielectric properties assigned to the ceramic disks and gel were taken from the manufacturer datasheet (see next section for values). To isolate the impedance of the fold from the total impedance of the model, we performed an additional simulation to determine the impedance of the disks and gels alone. For this purpose, a model including only two layers of gel sandwiched between

https://doi.org/10.5555/IEMP4633 ISSN 2488-8648

two ceramic disks of the same size as in the skin fold models was created. All simulations related to the simplified model were performed using Sim4Life v3.2 (ZMT Zurich MedTech AG). To generate current through the model, a constant voltage at 150kHz with an amplitude of 20 V was set to the outer surfaces of the disks. The total complex impedance of the models was then derived by first calculating the total current

$$A_{eff\,\mathrm{Re}} = \frac{1}{Z_{re}}\left(\frac{l_s}{\sigma_s} + 2\cdot\frac{l_d}{\sigma_d}\right)$$

(3.9)

$$A_{eff\,\mathrm{Im}} = \frac{1}{|Z_{\mathrm{Im}}|}\left(\frac{l_e}{\varepsilon_0\varepsilon_r\omega}\right).$$

(3.10)

flux passing through a plane parallel to the two ceramic disks and located between them, and then dividing the voltage between the two ceramic disks by the total current value. To calculate the effective cross-section of a skin fold from the real or the imaginary components of the complex impedance of the model, the following equations were used

Ttfields Simulations and Sensitivity Analysis

As part of this study, we performed numerical simulations of the delivery of TTFields to a realistic human computational phantom. These simulations were performed with three goals:

Simulations Setup

To simulate the delivery of TTFields to the abdomen, a realistic computerized model of a human male (DUKE 3.0 from ZMT) was used (Christ *et al*., 2010). The simulations were performed at 150kHz using Sim4Life v3.2 (ZMT) electro-quasi-static solver. Two TAs were placed on the phantom. Each array comprised 20 ceramic disks (20mm in diameter, 1mm thick), which made electric contact with the phantom skin through a thin layer of medical gel (20mm in diameter, 0.5mm thick). The TAs were placed on the back and on the stomach of the computational phantom using a semi-automatic algorithm reported elsewhere (Bomzon *et al*., 2015). As a baseline, all tissue properties were assigned to the phantom utilizing the IT'IS database 3.1.1 (Hasgall *et al.*, 2015), which is based on the Gabriel dispersion relationships (Gabriel ,1996). The values of skin, SAT, liver, and pancreas were then changed as described below. The dielectric properties of ceramic disks (σ = 0 S m−1, εr = 1000) and medical gels (σ = 0.1 S m−1, εr = 100) were obtained from the manufacturers' specification sheets. To deliver TTFields to the phantom, a constant voltage was imposed between the outer surfaces of the ceramic disks in the two TAs (Dirichlet boundary conditions). The voltage was normalized to simulate a current of 4A peak-to-peak flowing through the model. The model was voxelized with a maximum voxel size of 3mm3. To reduce computation time while minimizing errors, the model was truncated at the neck and below the waist of the phantom where the average electric field falls to 10% of its minimum value in the middle of the torso. It is worth noting that other human models and software simulation packages that could be suitable for studies such as this do exist. Information about other available human models and software simulation packages can be found in (Makarov *et al.*, 2017).

$$\varepsilon_{eff} = \frac{d_{skin}\,|Z_{\mathrm{Im}}|}{A\omega\,(Z_{\mathrm{Re}}^2 + Z_{\mathrm{Im}}^2)}\cdot\frac{1}{\varepsilon_0}$$

(3.11)

Applying Measured Dielectric Properties to the Computational Model

A challenge associated with applying the measured dielectric properties of the dermis and epidermis to the model is that in the computational phantom, skin is segmented as a single layer that does not reflect the electrical variability between the anatomical layers. Therefore, it is necessary to derive effective skin properties from the measured values such that the impedance of the phantom's single-layer skin will be equivalent to realistic two-layer skin impedance. This was done using the following equations:

https://doi.org/10.5555/IEMP4633 ISSN 2488-8648

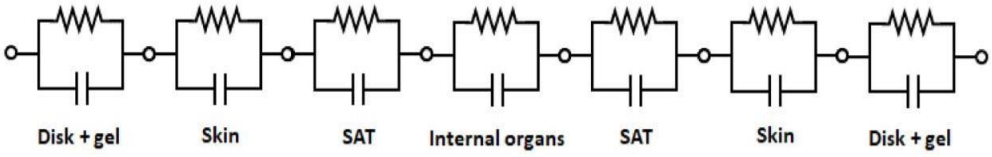

Fig 3 : Simplified electric circuit model of several resistor _capacitor units in series

representing TTFields delivery to the body. The different units represent ceramic disks attached to the body through medical gel, skin, and SAT layers and the internal organs

.

$$\sigma_{eff} = \frac{d_{skin} Z_{\mathrm{Re}}}{A\,(Z_{\mathrm{Re}}^2 + Z_{\mathrm{Im}}^2)}. \quad (3.12)$$

Here, ε0 is the vacuum permittivity, ω is the angular frequency, A is the cross-section of the electrodes, and dskin is the average skin thickness of the phantom. ZRe was calculated using equation (3.2) and the dermis conductivity extracted from the measurements. ZIm was calculated using equation (3.3) and the epidermis relative permittivity extracted from the measurements. For these calculations, the dermis thickness was taken as the average thickness of the phantom's skin, which was found by measuring the thickness of the skin at multiple sites
around the phantom's abdomen and then averaging these measurements. The epidermis thickness was considered to be 80 · 10−6 m, similar to the thickness used to derive the epidermis permittivity from the measurements. The cross-section A was taken to be the cross-section of the electrodes.

Sensitivity Analysis

For most biological tissues over the frequency range of 100 kHz–1 MHz, the conductivity has a stronger influence on the electric field and current density distribution than relative permittivity. Therefore, our major simulation sets tested the sensitivity of the computational phantom total impedance to the conductivity values assigned to the SAT and skin. We varied the conductivity of the skin from a low value of 0.0007 S m−1 (conductivity of dry skin reported in the Gabriel database (Hasgall *et al.*, 2015)) to a maximum value of 0.3 S m−1and varied the conductivity of the SAT between 0.04 S m−1 (fat conductivity in Gabriel database (Hasgall et al 2015)) and 0.45 S m−1.

In this analysis, the relative permittivity of the skin was set to either the nominal value derived from our measurements or to the values reported in the Gabriel database for dry and wet skin (1100 and 10 000, respectively). The relative permittivity of the SAT was set to 82 (Hasgall *et al*., 2015) in all simulations. The total impedance of the model was then calculated, and the differences resulting from the different settings were examined. Another set of simulations compared the contribution of the dielectric properties of the internal organs with the total impedance of the body versus the contribution of the outermost layers. In these simulations, skin and SAT were assigned with the dielectric values extracted from our measurements and the liver and pancreas were assigned with conductivity values that were either half or double the values in the Gabriel database (Hasgall *et al*.,2015). Finally, we tested the sensitivity of the electric field to all of the mentioned changes in dielectric properties by comparing the distribution of the field intensity in the pancreas for all settings. To gain additional insight into how the skin contributes to the total impedance of our models, we considered a simple electrical circuit representing the delivery of TTFields to the body. In this circuit, each tissue layer/component is represented as a resistor–capacitor unit, with all units connected in series, as shown in Figure 5. The center unit represents the internal organs of the body, which are sandwiched between units representing the outer body layers (skin and SAT) and the gels and disks comprising the TAs. To calculate the contribution of the skin unit to the total impedance of the body, we calculated ZRe and ZIm for the skin

https://doi.org/10.5555/IEMP4633 ISSN 2488-8648

$$Z_{\mathrm{Re}} = \frac{d\sigma}{(\sigma^2 + \varepsilon_0^2\varepsilon_r^2\omega^2)\,A} \quad (3.13)$$

$$Z_{\mathrm{Im}} = \frac{d\varepsilon_0\varepsilon_r\omega}{(\sigma^2 + \varepsilon_0^2\varepsilon_r^2\omega^2)\,A}. \quad (3.14)$$

Here, σ and εr are the conductivity and relative permittivity assigned to the phantom's skin in the simulations, ω is the angular frequency, d is the average thickness of the phantom's skin, and The total effective cross-section of the disks in a TA. This approximation is valid because the current in the skin just below the arrays is mostly concentrated in the regions under the disks before it spreads out in the torso volume. The absolute value of skin impedance was calculated for all skin properties used in the simulations and the contribution of the skin to the total impedance of the models was evaluated.

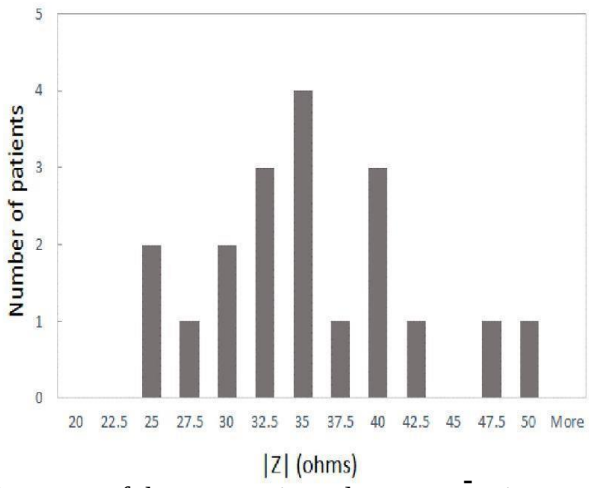

Figure 3.3 . Histogram of the average impedance per patient measured on 19 patients participating in the PANOVA trial(NCT01971281) during their first month of TTFields treatment.

Data Analysis and Discussion of Findings
Skin Models and Scaling Hierarchies

As already mentioned, the first macroscopic subdivision of skin happens according to the water content of the layers. It was found that for the model of intact skin with Skin cells a model down to the HYP is sufficient, i.e., the electric field does not penetrate beyond this layer. However, after removal of the rather insulating SC the penetration depth extends down to muscle tissue assuming a HYP thickness of 5 mm extracted from the MR image. Therefore, muscle is included in the model as well. The contribution of hair follicles, sweat glands and sebaceous glands mentioned in section 3.1 is not supposed to be negligible (especially the sweat ducts occasionally filled with sweat) but estimated to be more or less equal for all skin layers, leading to a certain but more or less equal offset in the dielectric properties. Furthermore, hair follicles and glands are not filled with cells and therefore not part of the presented model, because mainly the cells are observed to provide a significant contribution to the material dispersion in the lower MHz range. After defining the macroscopic model, the dielectric properties of each of the sublayers have to be defined. The complexity of the different models follows the subsequential inclusion of features that are likely to affect the dielectric spectrum.

In the MHz region the β-dispersion, the short-circuiting of the cell membranes is the dominant feature and has therefore to be reproduced by a valid model. Other dispersion mechanisms such as electrode

https://doi.org/10.5555/IEMP4633 ISSN 2488-8648

polarization and α-dispersion below 1 MHz and the relaxation of free water (γ dispersion) in the low GHz region occur outside of the considered frequency range. Therefore, those mechanisms are said not to affect the spectrum in the MHz range and are not included in the model. The weak δ-dispersion above 100 MHz caused by the relaxation of bound water and proteins might extend into the upper part of the frequency region of interest between 1 and 100 MHz, but is neglected here because of its weakness compared with the β-dispersion. Potential sources of error or variation are electrode surface roughness, the influence of a potentially occurring air or sweat layer or pressure variations and structural features crossing the entire skin (sweat ducts, hair follicles). However, the inclusion of trans-layer features is out of scope of this work.

Table 1. Overview of the skin models.

Model	Mixing formula	Number of phases per skin layer	Anisotropy
MGW	MG	2	No
MGI	MG	3 or more	No
LOI	LO	3 or more	No
MGA	MG	3 or more	Yes
HBA	HB	3 or more	Yes
NUM	Numerical (SC, E, HYP) and HB (D and M)	3 or more	Yes

Results of Sensitivity Analysis

The absolute value of impedance extracted from TTFields simulations with various combinations of dielectric properties for skin and SAT are presented in Table 1. Each column in the table is related to simulations performed with the same skin conductivity and each row is related to simulations performed with the same SAT conductivity. It is evident from Table 4.1 that assigning low conductivity and low permittivity to the skin (0.02 S m−1 and 1100, respectively) resulted in much higher impedances compared with all other combinations, regardless of SAT conductivity. In addition, for combinations with higher skin conductivity and/or permittivity, the total impedance did not change much.

Table 2. the absolute impedance of a model simulating the delivery of 150 kHz TTFields to the abdomen of a realistic human computational phantom using transducer arrays (20 disks each) placed on the phantom's abdomen and back with various dielectric properties assigned to the phantom's skin and SAT segments.

				|Z| (Ω)	
εr skin	σ skin (S m−1)/ σ SAT (S m−1)	0.02	0.07	0.11	0.3
1100	0.08	57	39	36	30
	0.2	53	36	33	28
	0.36	51	34	32	27
	0.45	50	34	31	27

https://doi.org/10.5555/IEMP4633 ISSN 2488-8648

5396	0.08	41	37	35	30
	0.2	37	35	32	28
	0.36	36	33	31	27
	0.45	35	32	30	26
10 000	0.08	36	35	34	30
	0.2	33	32	32	28
	0.36	32	31	30	27
	0.45	31	30	30	27

fill the entire torso volume, and current density at any point is significantly reduced. Consequently, changing the conductivity of a part of the internal volume has very little effect on the impedance of the entire volume. Therefore, the total impedance of the model was relatively insensitive to changes in the conductivity of specific organs.

The Effect of Skin Properties on Electric Field Intensity

The electric field intensities in the torso were extracted from all the simulations described in the sensitivity analysis after normalizing the current applied to the models to 4A peak to peak. Figures 8(a)–(d) show coronal and axial views of the electric field intensity in the abdomen (field amplitude) through the pancreas for simulations where skin and SAT properties were assigned with our nominal dielectric properties at 150 kHz and pancreas and liver conductivities were assigned with 50%, 100%, or 200% of their conductivity values as reported in the Gabriel database (Hasgall et al 2015). Intensity maps of all other combinations of dielectric properties for skin and SAT yielded very similar maps to figures 8(a) and (d), and therefore are not presented. Figure 8(e) shows a histogram plot of field intensities in the pancreas of the simulations mentioned above, as well as two in which extreme conductivity values were assigned to skin and SAT ([0.0007, 0.04] S m−1 and [0.45, 0.3] S m−1, respectively), and a simulation in which skin and SAT conductivity were set to nominal values and the current was set to 2A peak to peak. It is evident from Figure 8(e) that for a given current, the median electric field within the pancreas changed very little (less than about 10%), even when the skin and SAT properties changed by one and two orders of magnitude. However, changing the conductivity assigned to the pancreas had a significant influence on field intensity within this organ: the higher the conductivity, the lower the electric field. These results can be explained by examining the field intensity maps shown in Figure 4.1 Once the current penetrates the skin, it spreads out in the body, and only a small fraction of the current passes through any specific organ. Therefore, while changing the conductivity of a specific organ causes only small changes in the distribution of the current, changes in the electric field in that organ are proportional to the changes in conductivity. This is because the electric field intensity equals the unchanged current density divided by the conductivity.

Discussion

The purpose of this study was to elucidate the role of the outer-body layers (skin and SAT) in shaping the intensity and distribution of TTFields in the clinical setting by combining measurements with numerical simulations. The study comprised two parts: In the first part, we measured the dielectric properties of the skin under conditions similar to those imposed on the skin when delivering TTFields to patients with cancer. In the second part, we performed computational simulations to evaluate how the dielectric properties of the skin influence the intensity and distribution of TTFields. To measure the properties of the outer-body layers, we placed electrodes on either side of skin folds at several locations around the waists of volunteers and measured the impedance of the folds. Assuming that the tissue in the skin fold comprised three layers

https://doi.org/10.5555/IEMP4633 ISSN 2488-8648

(epidermis, dermis, and SAT) and analyzing the linear relationship between fold thickness and impedance, we derived dielectric properties for the three tissue types in the model. The calcu the fold using imaging modalities such as optical coherent tomography and high frequency ultrasound (Laurent *et al*.,2007, Sattler *et al*., 2013). For an electrical model to be considered representative of the subject it simulates, the total impedance of the model must match that of the subject. Since other methods for validation such as in vivo measurement of the electrical field or current within the subject are more complicated and often not feasible, at present, comparing total impedance may be the only practical method for testing the reliability of computational models simulating delivery of TTFields. Therefore, total body impedance was used to indicate that the dielectric properties of skin and SAT that we measured were representative of the dielectric properties of these tissues in patients treated with TTFields. For this purpose, we incorporated the measured dielectric properties into a realistic human computational phantom by calculating effective permittivity and conductivity for the single layer phantom skin, which generated an impedance equal to the impedance of a two-layer skin.

The effective skin conductivity and permittivity derived for the model (0.07 S m−1, εr = 5340 at 150kHz) are within the low range of values previously reported for skin (Wake et al 2016):

0.1 ± 0.017 S m−1, Gabriel wet skin: 0.094 ± 0.0131 S m−1, εr = 11362, Gabriel dry skin:

0.0007 ± 0.0001 S m−1, εr = 1111 (Gabriel *et al* .,1996c, Andreuccetti *et al*., 1997). The lower values derived from our measurements compared with wet skin may arise from the medical gel used in our study as a moistening agent versus the saline solution that was used in other studies.

The conductivity for SAT tissue derived from our study (0.2 S m−1) is in the higher range of conductivity reported by Wake et al (2016) (0.15 ± 0.02 S m−1) and is about 2.5 times higher than the conductivity reported for fat by Gabriel *et al.* (2009) (0.08 S m−1). These differences may be due to different origins of the skin samples and different water content in the samples used in the different studies, which are known to influence fat conductivity (Wake et al 2016). Differences in the composition of this layer and the relative volume fraction of connective tissue in the sample (conductivity of 0.39 S m−1 at 150kHz (Hasgall *et al*., 2015)) may also increase the measured conductivity of the discussed layer of interest. This suggests that the values extracted from our measurements are valid for the subcutaneous tissue layer in computational phantoms.

When we applied SAT conductivity and skin-effective dielectric properties to the phantom and simulated delivery of TTFields to the phantom abdomen, the total impedance of the model was within the mid-range of values measured on patients. In previous studies involving TTFields delivery to the abdomen, lower conductivity values were assigned to the skin and SAT (0.02 S m−1 and 0.08 S m−1, respectively). The typical impedance of the models in these studies was around 57 Ω, which is in the higher range of impedance measured on patients. Thus, the conductivity values derived in this study yield a better representation of the average patient treated with TTFields than the conductivity values used in previous studies. Of note, the impedance measured on a single patient may vary by more than 10 Ω over a single month. It is unlikely that this large variation arises from changes in the resistivity of the internal organs and tissues; it most likely originates from changes in skin conductivity and contact between the arrays and the skin. Understanding the exact causes for this variation is beyond the scope of this study and may be examined in detail in future studies. The second part of this study focused on a sensitivity analysis in which we examined the degree to which variations in the dielectric properties of skin and SAT influenced the model impedance and field intensity of TTFields delivered to computational phantoms. We showed that skin properties contributed significantly to the total model impedance when they were below a threshold value of about 0.05 S m−1 and a relative permittivity of 5000. However, once they exceed these values, skin impedance drops to a level where it is small relative to the impedance of the rest of the body, and the total impedance of the body is insensitive to further increases in these properties. The dielectric properties we measured for skin and SAT placed these layers in the region where their contribution to the overall impedance was small relative to the contribution of the inner-body tissues. Therefore, our body model was relatively insensitive to the dielectric properties of these layers, and even an increase of over 100% in skin and SAT dielectric properties due to inaccuracies in the measurements or realistic physiological changes that may increase skin conductivity may not be reflected in measurements of the total body impedance. In this context, it is interesting to note that according to our simulations, for a given current applied to the TAs, the field distribution within key organs (liver and pancreas) was only affected minimally by skin conductivity, even when the conductivity was below the threshold. This is because the current flowing through any plane crossing the body between the TAs is equal to the applied current

regardless of skin properties. Thus, the current density in different regions of the body is largely unaffected by skin conductivity. Since the electric field is proportional to the current density, it is also mostly unaffected by skin conductivity. However, since the electric field intensity in any material is inversely proportional to its conductivity, field intensities within the organs are highly sensitive to the organs' conductivities, as shown in this study. In addition, applying higher currents results in higher electric fields. Therefore, when studying TTFields distribution within the body, accurate determination of the skin properties is only of secondary importance relative to accurately setting the properties of the organs of interest. In particular, the field intensity within tumors will strongly depend on the electric properties of the tumor and its surrounding tissues. Since reliable information on the electric properties of tumors in the frequency range of 100Hz–1 MHz is scarce, studies focusing on measuring tumor properties within this range are warranted.

Conclusions

The study looked into how to calculate the skin's effective dielectric constant numerically. This work is a thorough investigation of the dielectric characteristics of skin and SAT in environments that are comparable to those that patients' skin must endure when receiving tumor-treating fields (TTFields). The results of this study have implications for many other low-frequency electrotherapeutics, including neurostimulation and electric muscle stimulation. To determine the dielectric characteristics of skin and SAT, this study integrated models and experimental data. Next, it was investigated how these characteristics affected the distribution of TTFields throughout the body as well as the total body impedance. The total impedance of the computational models matched patient data well when the measured dielectric properties were applied to simulate the delivery of TTFields to patients. This suggests that the skin and SAT dielectric properties reported in this study should be used as standard values in future research on the delivery of TTFields to the torso. Furthermore, our findings imply that the skin's and SAT's dielectric characteristics fall within an area where they largely affect the distribution of the electric field inside the body as well as the total impedance of bodies to which TTFields are applied.

References

Andreuccetti, D., Biagi, P.F. and Giannetti, G. (1997). A numerical model of the human body for anatomically realistic electric field dosimetry. *Physics in Medicine* and *Biology*, 42(3), 479–490.

Bomzon, Z., Rubinstein, J.T. and Tabor, E. (2015). Theoretical and numerical analysis of electrode-tissue contact and activation properties in spinal cord stimulation. Neuromodulation: *Technology at the Neural Interface*, 18(6), 466–476.

Christ, A., Samaras, T. and Neufeld, E. (2010). Age-dependent tissue-specific exposure of cell phone users. *Physics in Medicine andBiology*, 55(7), 1763–1783.

Cowen, S.A., Milnes, P. and Sazonov, A. (2014). 3D numerical model of human ventricular activation and electrogram dynamics. *Journal of Electrocardiology*, 47(6), 895–901.

Davies, B. R., Cooley, J.W.and Troup, G.J. (2013). Simulating human electroencephalography (EEG) responses using a coupled finite element model of the head and a neural mass model. *NeuroImage*, 75, 240–247.

Gabriel, C., Peyman, A., andGrant, E.H. (1996). Electrical conductivity of tissue at frequencies below 1 MHz. *Physics in Medicine andBiology*, 41(11), 2251–2269.

Gabriel, C., Gabriel, S., and Corthout, E. (2016). The dielectric properties of biological tissues: III. Parametric models for the dielectric spectrum of tissues. *Physics in Medicine and Biology*, 41(11), 2271–2293.

Giladi, M., Porat, N., and Amos, O. (2014). Novel electrode configurations for effective deep brain stimulation. *IEEE Transactions on Biomedical Engineering*, 61(2), 498–505.

Giladi, M., Porat, N., and Amos, O. (2015). Impact of electrode geometry on electrical field distribution in deep brain stimulation. *Brain Stimulation*, 8(5), 1063–1069.

Hasgall, P.A., Neufeld, E and Gosselin, M.C. (2015). IT'IS Database for thermal and electromagnetic parameters of biological tissues. Version 3.0. Zurich: Foundation for Research on Information Technologies in Society.

Huclova, S., Rydlo, J. and Kania, M. (2010). Calculation of electric field in human tissues from contact current exposure in domestic and occupational

https://doi.org/10.5555/IEMP4633 ISSN 2488-8648

environments. *IEEE Transactions on Magnetics*, 46(8), 3048–3051.

Karanam, S.A., Poole, M.S., and Witzke, E.L. (2017). Electromagnetic modeling of coil and lead configurations for deep brain stimulation. *Brain Stimulation*, 10(3), 634–642.

Kirson, E.D., Gurvich, Z., and Schneiderman, R. (2007). Disruption of cancer cell replication by alternating electric fields. *Cancer Research*, 64(9), 3288–3295.

Laurent, R., Stoppa, D., and Rebai, M. (2007). Numerical computation of the electric field produced by a HVDC underground cable. *IEEE Transactions on Magnetics*, 43(4), 1372–1375.

Otaki, H., Abundes, R. and Shoji, K. (2017). Numerical analysis of electromagnetic fields in the human body under 50/60 Hz power line condition. *IEEE Transactions on Magnetics*, 53(2), 1–6.

Sattler, J., Schlattner, U. and Otten, U. (2013). Adult hippocampal neurogenesis: Regulation and possible functional and clinical correlates. Frontiers in Neuroanatomy, 7, 1–19.

Voloshin, A.S., Kriegsmann, M. and Hancock, D.G. (2016). Numerical computation of skin depth and effective dielectric constant in layered biological tissues. *IEEE Transactions on Biomedical Engineering*, 63(9), 1793–1801.

Wake, K., Nudo, S. and Shibamoto, Y. (2016). Numerical analysis of electromagnetic waves through complex biological structures. *Progress in Electromagnetic Research*, 154, 89–97.